Journal of Physics: Conference Series **628** (2015) 012084 doi:10.1088/1742-6596/628/1/012084

A new angular resampling algorithm for the bearing fault diagnosis under the time-varying rotational speed

Tianyang Wang[1], Weidong Cheng[2], Jianyong Li[2], Fulei Chu[1]
[1]Department of Mechanical Engineering, Tsinghua University, Beijing 100084, China
[2]School of Mechanical Electronic and Control Engineering, Beijing Jiaotong University, Beijing 100044, China

E-mail: wty19850925@126.com

Abstract: Order tracking is one of the most effective algorithms to eliminate the effect of time-varying rotational speed on the rotary machines. However, this algorithm is not suitable for the faulty rolling bearing unless the peak time of the fault-induced impulse is set as zero which cannot be met in the real engineering. The traditional resampling process will cause uneven intervals between the adjacent impulse peaks in the angular domain and then affect the envelope analysis-based diagnosis result. To solve this problem, a new resampling algorithm with three parts is proposed: (a) linearly fitting the instantaneous rotational speed measured by the tachometer, (b) resampling the vibration signal from the time domain to the angular domain using the traditional method, (c) calculating the envelope deformation amount and then compensating the resampled result. The effectiveness of the proposed method has been validated by both the simulated and experimental bearing vibration signals.

1. Introduction

Rolling element bearings have been widely used in different rotating equipment. Reliable bearing conditional monitoring is crucial to avoid the failure or degraded performance of the whole machine [1]. In real engineering, the bearings always operate under time-varying speed which will then make the bearing vibration signal non-stationary and the techniques based on the assumption of constant rotating speed inapplicable [2, 3]. To solve this problem, the order tracking algorithm was proposed to remove the effects of speed fluctuation and smearing of the spectrum by resampling the original vibration signal at a constant angle increment and converting the non-stationary signal in time domain into the stationary one in angular domain [4-6].

However, when the resampling algorithm is used to analysis the rolling bearing with time-varying rotational speed, it will cause the envelope deformation [7] which may then effect the final bearing

fault diagnosis. To solve this problem, a new resampling algorithm is proposed to compensate the deformation. At first, the distribution character of the peak time under the time-varying rotational speed is deduced. The rules of envelope deformation is then summarized based on the analysis in [7]. And the new resampling algorithm based on the piecewise fitting and envelope deformation compensation is finally put forward.

The rest of the paper is organized as follows: Section 2 deduces the distribution character of peak time of bearing fault-induced impulse and presents the rules of envelope deformation caused by the traditional angular resample algorithm. Section 3 presents the new resampling method. Section 4 and 5 examine the performance of the new resampling algorithm using the simulated and experimental data respectively. The conclusions are drawn in Section 6.

2. The principle of envelope deformation

As proposed in [7], the envelope deformation happens when the traditional angular resampling algorithm is used to analysis the faulty rolling bearing signal under the time-varying rotational speed. And the essential reason of this phenomenon is the existence of peak time and the corresponding effect on the traditional angular resampling algorithm. The distribution character of the peak time under time-varying rotational speed is firstly obtained, and the envelope deformation rule is then presents with the assumption of the constant peak time.

2.1 The distribution character of the peak time

In general, when a rolling element bearing has a local fault, the contact between the defect and its mating surface will generate an impulse with a short duration in which the peak time (t_p) is defined as the time interval between the starting point and the maximum value. In this section, the real response of the bearing fault impulse is simulated with the time response of the undamped spring-mass system to a half sine wave excitation. Eq. (1) represents the impulse and the corresponding response can be divided into two phase: load stage ($0 < t < T=\pi/\omega$) and unload stage ($t > T=\pi/\omega$).

$$F(t)=\begin{cases} P_0 \sin \omega t (0<t<T=\pi/\omega) \\ 0(\text{others}) \end{cases} \tag{1}$$

where T and ω are the duration time and the angular frequency. Using the Duhamel's integral, the peak time can be expressed:

$$t_p=\begin{cases} \dfrac{\pi}{2}\left(\dfrac{2p+1}{\omega_n}-\dfrac{1}{\omega}\right)(\omega>\omega_n) \\ \dfrac{2p\pi}{\omega_n+\omega}(\omega<\omega_n) \end{cases} \quad (p=1,2,\mathrm{L}) \tag{2}$$

According to the Eq. (2), if the ω is bigger than the ω_n, the load time is relatively small. So the maximum value happens after the load time. On the contrary, if the ω is smaller than the ω_n, the peak value happens before the load time. To evaluate the distribution character of peak time under time-varying speed, the parameters in Eq. (2) should be given. The ω can be expressed by the rolling bearing parameters:

$$\omega=\frac{\pi}{T}=\frac{\pi}{l_{fault}/v_{line}}=\frac{\pi}{l_{fault}/(\omega_{bearing}\times\pi\times d_{pitch})} \tag{3}$$

where, l_{faul} is width of local fault; v_{line} is the linear velocity fault point; $\omega_{bearing}$ is the rotational frequency of the rolling bearing; d_{pitch} is the corresponding pitch diameter. So, the Eq. (2) can be expressed by:

$$t_p=\begin{cases}\frac{\pi}{2}\left(\frac{2p+1}{\omega_n}-\left(\frac{\pi}{l_{fault}/(\omega_{bearing}\times\pi\times d_{pitch})}\right)^{-1}\right)\left(\omega_n<\frac{\pi}{l_{fault}/(\omega_{bearing}\times\pi\times d_{pitch})}\right)\\ 2p\pi\left(\omega_n+\frac{\pi}{l_{fault}/(\omega_{bearing}\times\pi\times d_{pitch})}\right)^{-1}\left(\omega_n>\frac{\pi}{l_{fault}/(\omega_{bearing}\times\pi\times d_{pitch})}\right)\end{cases}(p=1,2,\mathrm{L}) \tag{4}$$

Without loss of generality, the specific value of all the parameters in Eq. (4) are set as follow: the higher resonance frequency is set as 10000Hz, the varying range of the rotational speed is set as an extremely wide interval of [0 10000Hz], p, d_{pitch} and l_{fault} are separately set as 1, 33.5 mm and 1 mm.

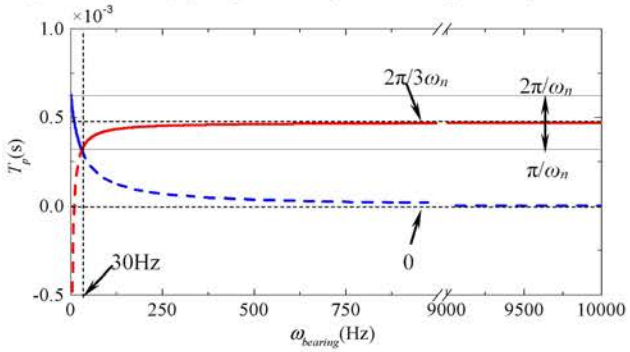

Figure 1. The rule of peak time changing with bearing rotational frequency

In Fig. 1, The blue line and red line separately represent the first and the second expression of Eq.(4). And the solid part represents the real change law of the peak time. In this way, the peak time actually changes in the interval of $[\pi/\omega_n, 2\pi/\omega_n]$. Considering the resonance frequency ω_n is relative high, the corresponding value range are usually narrow. As for the simulation mentioned above, the specific value range is $[3.14\times10^{-4}, 6.28\times10^{-4}]$ which is extremely narrow. Based on the aforementioned analysis, we assume the peak time as a constant value with the time-varying rotational speed.

2.2 The presentation of the envelope deformation phenomenon

If the peak time can be considered as a constant value with the time-varying bearing rotational speed, the peak times at the higher rotational speed will be lengthened more significant than the one at lower rotational speed in the angular domain using the traditional resampling algorithm. This phenomenon of unequally spaced peaks is called envelope deformation which will then affect the envelope spectrum and the fault diagnosis of rolling bearing. In this subsection, an analytical model is constructed to specify this kind of the envelope deformation where the half-sine wave is used to simplify the fault-induced impulse, and the projection of the ascending segment on the base is the peak time. Fig. 2(a) is the schematic diagram of envelope deformation theory using the simulated signal of faulty rolling bearing with a constant accelerator. $t_{1,s}$, $t_{2,s}$ and $t_{3,s}$ are the start moments of the adjacent three

impulses, $t_{1,p}$, $t_{2,p}$ and $t_{3,p}$ are the peak moments. Just because the peak time does not change with rotational speed, $t_{1,p}$ - $t_{1,s}$, $t_{2,p}$ - $t_{2,s}$ and $t_{3,s}$ - $t_{3,p}$ should equal to each other. Fig. 2(b) is the resampled angular waveform, in which $\varphi_{1,s}$, $\varphi_{2,s}$ and $\varphi_{3,s}$ are the corresponding start phases, $\varphi_{1,p}$, $\varphi_{2,p}$ and $\varphi_{3,p}$ are the peak phases. In the angular domain, the start phases are equally spaced ($\Delta\varphi_{s,2}=\Delta\varphi_{s,3}/2$), however, the peak phases are not.($\varphi_{1,p}$ - $\varphi_{1,s} \neq \varphi_{2,p} - \varphi_{2,s} \neq \varphi_{3,p} - \varphi_{3,s}$).

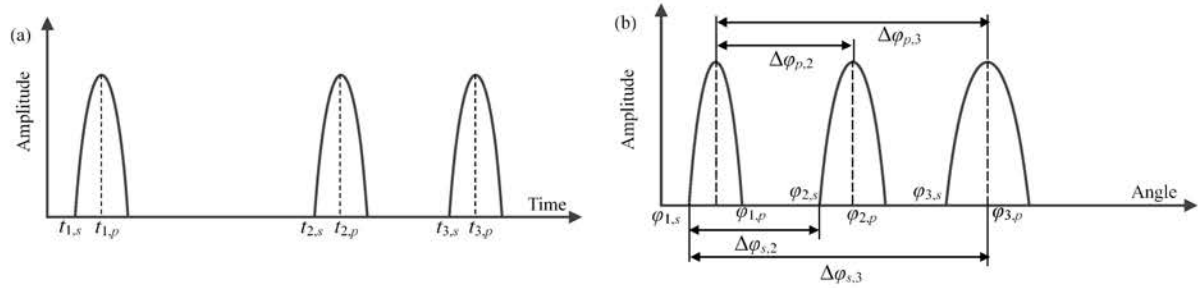

Figure 2. The schematic diagram of envelope deformation theory: (a) time-domain waveform with rotational speed up; (b) outcome of angular resample

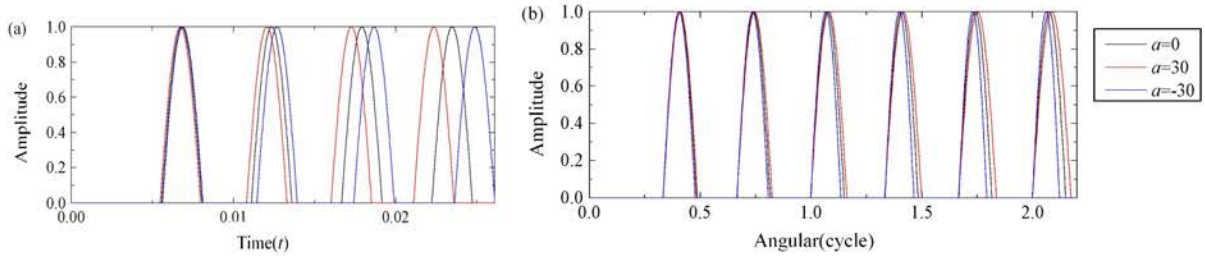

Figure 3. The schematic diagram of the envelope deformation: (a) the waveform of simulated faulty bearing vibration; (b) the angular resampling outcome using traditional order tracking algorithm

Figure 3 gives examples to visualize the envelope deformation. In Fig. 3(a), the black line represents the signal with a constant rotational speed and the red and blue signals are separately speed-up and speed-down signal with the acceleration of 30 and -30. As for the resampled results in the angular domain shown in Fig 3(b), we can see that the start phases of all the impulses are equally spaced and the peak phases are not which can be used to testify the existence of the envelope deformation.

Fig 4(a) and (b) are the corresponding order spectrums of the speed up and speed down situations. The theoretical positions of the fault characteristic frequency and its harmonics are '3', '6' and '9' which are displayed by vertical dash lines. As shown in Fig. 4(a) and Fig. 4(b), the peaks will both deviate from their theoretical positions. This can prove that the tradition angular resampling algorithm will the envelope deformation will then affect the rolling bearing fault diagnosis

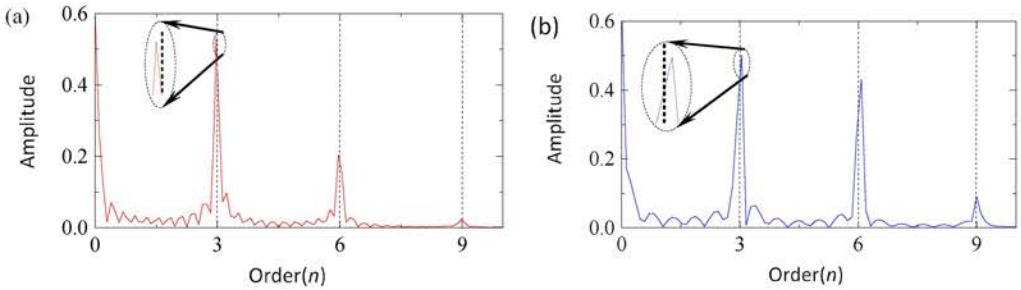

Figure 4. The order spectrums of simulated faulty bearing vibration signal under different laws of time-varying rotational speed: (a) positive acceleration; (b) negative acceleration

3. The revised angular resampling algorithm

As mentioned in [7], the relative deformation value of the *n*th impulse is listed as follow:

$$\Delta\varphi_{1,n} = (\varphi_{n,p} - \varphi_{n,s}) - (\varphi_{1,p} - \varphi_{1,s}) = (2an\Delta\varphi_s + n_{1,s}^2)^{1/2} - n_{1,s})\, t_p \tag{5}$$

where, $\varphi_{n,s}$ and $\varphi_{n,p}$ are separately the start phase and the peak phase of the nth impulse, $\varphi_{1,s}$ and $\varphi_{1,p}$ are the start phase and the peak phase of the first impulse, a is the acceleration , $n_{1,s}$ is the initial rotational speed, t_p is the peak time. Following Eq. (5), Table 1 gives the peak phases and the corresponding relative deformation value:

Table 1: The peak angle and relative deformation of the impulse waveforms

	Peak phase	Relatively deformation
The first impulse	$\varphi_{1,s} + n_{1,s} \cdot t_p + \frac{1}{2}at_p^2$	0
The second impulse	$\varphi_{1,s} + \Delta\varphi_s + (2a\Delta\varphi_s + n_{1,s}^2)^{1/2} t_p + \frac{1}{2}at_p^2$	$(2a\Delta\varphi_s + n_{1,s}^2)^{1/2} - n_{1,s})\, t_p$
The *n*th impulse	$\varphi_{1,s} + (n-1)\Delta\varphi_s + (2a((n-1)\Delta\varphi_s) + n_{1,s}^2)^{1/2} t_p + \frac{1}{2}at_p^2$	$(2a(n-1)\Delta\varphi_s + n_{1,s}^2)^{1/2} - n_{1,s})\, t_p$
The *n*+1th impulse	$\varphi_{1,s} + (n)\Delta\varphi_s + (2a(n)\Delta\varphi_s + n_{1,s}^2)^{1/2} t_p + \frac{1}{2}at_p^2$	$(2a(n\Delta\varphi_s) + n_{1,s}^2)^{1/2} - n_{1,s})\, t_p$

According to the peak phases and relatively deformation values listed in Table 1, it is found that if we subtract the relatively deformation value from the corresponding peak time, the adjusted peak time are equally spaced. $\Delta\varphi'_{n+1,n}$ is the phase interval between the adjusted *n*th phase peak and the *n*+1th phase peak.

$$\begin{aligned}\Delta\varphi'_{n+1,n} &= \varphi'_{n+1,p} - \varphi'_{n,p} = (\varphi_{n+1,p} - \Delta\varphi_{1,n+1}) - (\varphi_{n,p} - \Delta\varphi_{1,n}) \\ &= (\varphi_{1,s} + n_{1,s} \cdot t_p + \frac{1}{2}at_p^2 + n\Delta\varphi_s) - (\varphi_{1,s} + n_{1,s}t_p + \frac{1}{2}at_p^2 + (n\text{-}1)\Delta\varphi_s) = \Delta\varphi_s\end{aligned} \tag{6}$$

As shown in Eq. (6), the phase interval after compensation become a constant value. In this way, the aforementioned envelope deformation phenomenon can be compensated by subtracting the relative deformation value from the x-axis of resampled angular waveform. In this paper, we call it the ideal compensation value. In real application, this ideal compensation value can be rewritten as follow:

$$\varphi_{c,i}=(\ (2(a(n-1)\Delta\varphi_s)+n_{1,s}^2)^{1/2}-n_{1,s})\,t_p=(\ (2a_i\Delta\varphi_i+n_b^2)^{1/2}-n_b)\,t_p \tag{7}$$

where, $\varphi_{c,i}$ is the compensation value of angular i in angular domain, a_i is the corresponding acceleration, $\Delta\varphi_i$ is angle the rolling bearing has rotated, n_b is the initial rotational speed.

The a_i and t_p can be determined by Eq. (8) and (9)

$$a_i=\frac{IF_{i+1}-IF_i}{\Delta t} \tag{8}$$

$$t_p=\frac{3\pi}{2\omega_n} \tag{9}$$

where, IF_{i+1} and IF_i are the corresponding instantaneous rotational speed measures by the speed sensor. The value of t_p is the mean of interval of $[\pi/\omega_n, 2\pi/\omega_n]$ mentioned in section 2.1. ω_n is the resonance frequency whose value can be determined by the kurtogram-based spectrum kurtosis[8-10].

Above all, the revised resampled algorithm is presented as follow:

STEP 1: Determine the variation trend of IF piecewise.

According to the number of the discrete IFs measured by the speed sensor, the raw signal is divided into n segments. We assume the acceleration of every segment as a constant value a_i ($0 < i < n$-1), the IF in every segment can be expressed by:

$$\mathrm{IF}(t)=k_i t+b_i\left(\frac{T}{n-1}(i-1)<t<\frac{T}{n-1}i\right) \tag{10}$$

where, T is the time duration of the signal, n is the number of the segments, k_i and b_i are the coefficients.

STEP 2: Determine the angular axis of every time-domain sampled point in angular domain.

$$\mathrm{Angle}(t)=\sum_{i=1}^{k}\frac{T}{2(n\text{-}1)}(\mathrm{IF}(i)+\mathrm{IF}(i+1))+\int_{\frac{T}{n\text{-}1}k}^{t-\frac{T}{n\text{-}1}k}a_{k+1}t+b_{k+1}dt \tag{11}$$

where k is the number of the segments before t.

STEP 3: Calculate the compensation value.

$$\begin{aligned}\mathrm{Angle}_c(t)&=(\ (2a_i\Delta\varphi_i+n_b^2)^{1/2}-n_b)\,t_p\\&=(\ (2\frac{IF_i-IF_{i-1}}{T/(n\text{-}1)}\mathrm{Angle}(t)+IF^2(1))^{1/2}-IF(1))\frac{2\pi}{3\omega_n}((\frac{T}{n\text{-}1}(i-1)<t<\frac{T}{n\text{-}1}i))\end{aligned} \tag{12}$$

STEP 4: Compensate the envelope deformation.

$$\mathrm{Angle}'(t)=\mathrm{Angle}(t)-\mathrm{Angle}_c(t) \tag{13}$$

STEP 5: Determine the sample points in the angular domain.

$$\frac{f_s}{\mathrm{IF}_{base}}:\frac{f_s}{\mathrm{IF}_{base}}:\sum_{i=1}^{n\text{-}1}\frac{T}{2(n\text{-}1)}(\mathrm{IF}(i)+\mathrm{IF}(i+1)) \tag{14}$$

where f_s/IF_{base} is the sample rate of the angular domain, IF_{base} is minimum of the measured IF.

STEP 6: Complete the resample process using the interpolation algorithm.

4. Simulation analyses

In this section, the simulated signal in Fig. 3(a) are used to testify the effectiveness of the propose algorithm. In specific, the change rules of the red and blue are separately $f(t)=30t+20$ and $f(t)=-30t+20$. Fig. 5 and Fig. 6 show the results using the algorithm described in Section 3. Fig. 5(a) and 6(a) are the compensation values; Fig. 5(b) and 6(b) are the corresponding envelope spectrum. It is obvious that the peaks representing fault characteristic frequency and corresponding harmonics in Fig. 5(b) and 6(b) are all compensated to its theoretical values, '3', '6' and '9'. It is proved that the revised angular resampled algorithm are effective both under speed up and speed down situations.

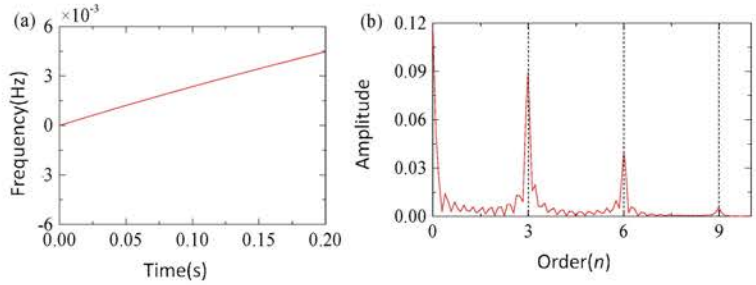

Figure 5. Speed-up model: (a) the compensation values; (b) the order envelope spectrum

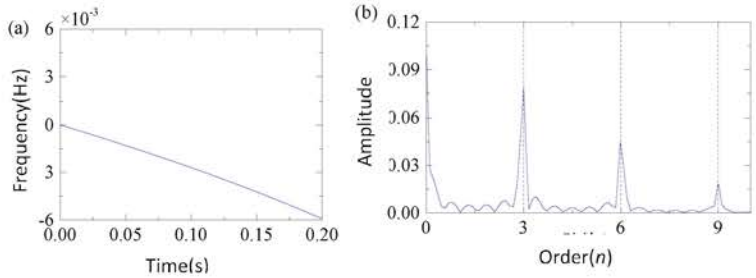

Figure 6. Speed-down model: (a) the compensation values; (b) the order envelope spectrum

5. Experimental tests

The effectiveness of the proposed algorithm is further tested using a set of experimental bearing vibration signals with fault in the outer race.

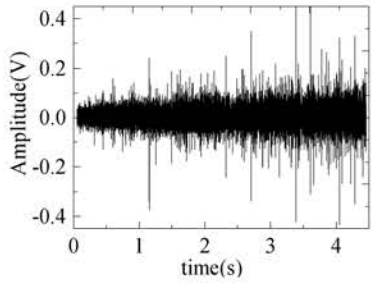

Figure 7. Raw signal with the increasing speed

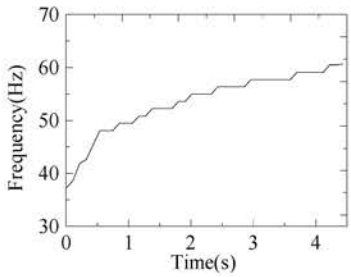

Figure 8. The measured IF of the rolling bearing

The corresponding rotational frequency of the rolling bearing increases from 38 Hz to 60 Hz. The sampling rate is 24,000 samples/s. The type of rolling bearing is ER16K, the fault characteristic

frequency equals to 3.45×f_r. The data lasts for 4.3 s. Fig. 7 and Fig. 8 are separately the waveform and the corresponding IF. Fig. 9 shows the resampled waveform using the revised resampling algorithm and the corresponding order envelops spectrum is shown in Fig.10. For comparison, Fig. 11 shows the order envelope spectrum using the traditional resampling algorithm. In Fig. 10 and 11, there both exist three vertical dash lines which represent theoretical fault characteristic frequency and its second and third harmonics. Their x-axis coordinates are 3.45, 6.9 and 10.35.

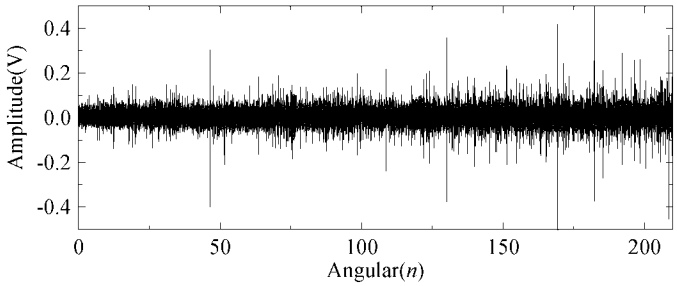

Figure 9. The resampled waveform using the revised resampling algorithm

It is obvious that the peaks representing the fault characteristic frequency and its harmonics in Fig 11 are not on their theoretical value. In Fig. 10, the revised resampling algorithm can compensate the envelope deformation and the corresponding fault characteristic order and harmonics are all adjusted to the theoretical value. This can testify the effectiveness of the proposed algorithm.

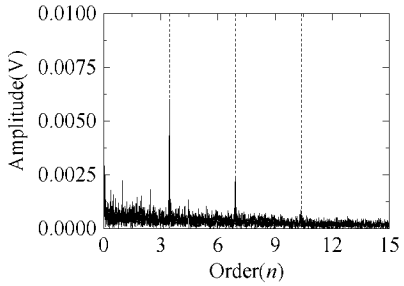

Figure 10. The order envelope spectrum using the revised resampling algorithm

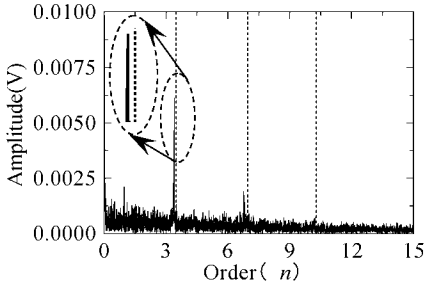

Figure 11. The order envelope spectrum using the traditional resampling algorithm

6. Conclusions

A revised resampling algorithm has been proposed to deal with the envelope deformation phenomenon caused by the traditional resampling algorithm. And the corresponding order envelope spectrums are more accurate than the ones obtained using traditional resampling algorithm. It is proved that this revised resampling algorithm is effectiveness under both the speed up and speed down situations.

Acknowledgments

The research work described in this paper was supported by Natural Science Foundation of China under Grant no.51335006 and Beijing Natural Science Foundation under Grant no.3131002.

References:

[1]. R B Randall and J Antoni 2001 Rolling element bearing diagnostics—a tutorial *Mechanical system signal processing* **25** 485

[2]. McFadden P D and J D Smith 1984 Vibration monitoring of rolling element bearings by the high-frequency resonance technique-a review *Tribology international* **17** 3

[3]. Wang T Y, Liang M, Li J Y and Cheng W D 2014 Rolling element bearing fault diagnosis via fault characteristic order (FCO) analysis *Mechanical system signal processing* **45** 139

[4]. Borghesani P, Ricci R, Chatterton S, and Pennacchi P 2013 A new procedure for using envelope analysis for rolling element bearing diagnostics in variable operating conditions, *Mechanical system signal processing* **38** 23

[5]. Gao Y, Guo Y, Chi Y L, Qin S R 2006 Order Tracking Based on robust peak search instantaneous frequency estimation. *J. Phys.: Conf. Ser* **48** 479

[6]. Fyfe K R and E D S Munck 1997 Analysis of computed order tracking *Mechanical system signal processing* **11** 187

[7]. Cheng W D, Gao R X, Wang J J, Wang T Y, Wen W G and Li J Y 2014 Envelope deformation in computed order tracking and error in order analysis *Mechanical system signal processing* **48** 92

[8]. Antoni J 2007 Fast computation of the kurtogram for the detection of transient faults *Mechanical system signal processing* **21** 108

[9]. Antoni J 2006 The spectral kurtosis: a useful tool for characterizing non-stationary signals, *Mechanical system signal processing* **20** 282

[10]. Antoni J and R B Randall 2006 The spectral kurtosis: application to the vibratory surveillance and diagnostics of rotating machines *Mechanical system signal processing* **20** 308